

Journal of Visualized Experiments

Deep vascular imaging in the eye with flow-enhanced ultrasound

--Manuscript Draft--

Article Type:	Invited Methods Collection - JoVE Produced Video
Manuscript Number:	JoVE62986R2
Full Title:	Deep vascular imaging in the eye with flow-enhanced ultrasound
Corresponding Author:	Christian Damsgaard Aarhus University: Aarhus Universitet Aarhus C, NA DENMARK
Corresponding Author's Institution:	Aarhus University: Aarhus Universitet
Corresponding Author E-Mail:	christian.damsgaard@aias.au.dk
Order of Authors:	Christian Damsgaard Henrik Lauridsen
Additional Information:	
Question	Response
Please specify the section of the submitted manuscript.	Biology
Please indicate whether this article will be Standard Access or Open Access.	Standard Access (\$1400)
Please indicate the city, state/province, and country where this article will be filmed . Please do not use abbreviations.	Aarhus, Denmark
Please confirm that you have read and agree to the terms and conditions of the author license agreement that applies below:	I agree to the Author License Agreement
Please provide any comments to the journal here.	
Please confirm that you have read and agree to the terms and conditions of the video release that applies below:	I agree to the Video Release

TITLE

Deep Vascular Imaging in the Eye with Flow-Enhanced Ultrasound

AUTHORS AND AFFILIATIONS

Christian Damsgaard^{1,2}, Henrik Lauridsen^{3,*}

¹Aarhus Institute of Advanced Studies, Aarhus University, Høegh Guldbergsgade 6B, 8000 Aarhus C, Denmark

²Zoophysiology, Department of Biology, Aarhus University, C. F. Møllers Alle 3, 8000 Aarhus C, Denmark

³Department of Clinical Medicine, Aarhus University, Palle Juul-Jensens Boulevard 99, 8200 Aarhus N, Denmark

Email addresses of co-authors:

Christian Damsgaard (christian.damsgaard@aias.au.dk)

Henrik Lauridsen (henrik@clin.au.dk)

*Corresponding author:

Henrik Lauridsen (henrik@clin.au.dk)

SUMMARY:

We present a non-invasive ultrasound technique for generating three-dimensional angiographies in the eye without the use of contrast agents.

ABSTRACT:

The retina within the eye is one of the most energy-demanding tissues in the body and thus requires high rates of oxygen delivery from a rich blood supply. The capillary lamina of the choroid lines the outer surface of the retina and is the dominating source of oxygen in most vertebrate retinas. However, this vascular bed is challenging to image with traditional optical techniques due to its position behind the highly light-absorbing retina. Here we describe a high-frequency ultrasound technique with subsequent flow-enhancement to image deep vascular beds (0.5–3 cm) of the eye with a high spatiotemporal resolution. This non-invasive method works well in species with nucleated red blood cells (non-mammalian and fetal animal models). It allows for the generation of non-invasive three-dimensional angiographies without the use of contrast agents independent of blood flow angles with a higher sensitivity than Doppler-based ultrasound imaging techniques.

INTRODUCTION:

The high metabolism on the vertebrate retina imposes an intrinsic tradeoff between two contrasting needs; high blood flow rates and a light path devoid of blood vessels. To avoid visual disturbance of perfusing red blood cells, the retina of all vertebrates receives oxygen and nutrients via a sheet of capillaries behind the photoreceptors, the choriocapillaris^{1–3}. However, this single source of nutrients and oxygen imposes a diffusion limitation to the thickness of the retina^{4,5}, so many visually active species possess a variety of elaborate vascular networks to

provide additional blood supply to this metabolically active organ⁶. These vascular beds include blood vessels perfusing the internal retinal layers in mammals and some fishes^{4,7–10}, blood vessels on the inner (light-facing) side of the retina found in many fishes, reptiles, and birds^{4,11–13}, and countercurrent vascular arrangements of the fish choroid, the choroid *rete mirabile*, that allows for the generation of super-atmospheric oxygen partial pressures^{14–20}. Despite that these additional non-choroidal paths for retinal nutrient supply play an essential role in fueling the metabolic requirements of superior vision⁴, the three-dimensional anatomy of these vascular structures is poorly understood, limiting our understanding of the morphological evolution of the vertebrate eye.

Traditionally, retinal blood supply has been studied using optical techniques, such as fundus ophthalmoscopy. This category of techniques provides high-throughput non-destructive information on non-choroidal blood vessel anatomy in high-resolution²¹ and is therefore readily used in clinical diagnosis of abnormalities in retinal vessel structure²². However, the retinal pigment epithelium absorbs the transmitted light and limits the depth of view in these optical techniques, providing reduced information on choroidal structure and function without the use of contrast agent²¹. Similar depth limitations are experienced in optical coherence tomography (OCT). This technique can generate high-resolution fundus angiographies using light waves at the technical expense of depth penetration²³, while the enhanced depth imaging OCT can visualize the choroid at the expense of retinal imaging quality²⁴. Magnetic resonance imaging overcomes the optical limitations of ophthalmoscopy and OCT and can map vascular layers in the retina, albeit at a low resolution²⁵. Histology and microcomputed tomography (μ CT) maintain the high-resolution of the optical techniques and provide information on whole-eye vascular morphology⁴, but both techniques require ocular sampling and are therefore not possible in the clinic or rare or endangered species. To overcome some of the limitations of these established retinal imaging techniques, the study here presents an ultrasound protocol on anesthetized animals, where blood movement is mapped *in silico* on a series of equally-spaced two-dimensional ultrasound scans spanning a whole eye by applying a comparable technique as described previously for embryonic and cardiovascular imaging^{26–28} and in OCT angiography²⁹. This approach allows for the generation of non-invasive three-dimensional deep ocular angiographies without using a contrast agent and opens up new avenues for mapping blood flow distribution within the eye across species.

PROTOCOL:

The protocol below was performed with permission from the Danish Inspectorate for Animal Experimentation within the Danish Ministry of Food, Agriculture, and Fisheries, Danish Veterinary and Food Administration (Permit number 2016-15-0201-00835).

1. Anesthesia and ultrasound medium

1.1. Anesthetize the research animal.

NOTE: Type and dose of appropriate anesthesia are highly species-dependent. In general,

immersion-based anesthetics such as MS-222 (ethyl 3-aminobenzoate methanesulfonic acid), benzocaine (ethyl 4-aminobenzoate), and propofol (2,6-diisopropyl phenol) are useful in fish and amphibians which readily absorb the anesthetic over gills or skin (e.g., 0.05 mg·L⁻¹ benzocaine in rainbow trout). A range of dissolved compounds that can be administered intravenously, intramuscularly, intraperitoneally is available for amniotes, as are gas-based anesthetics. Alfaxalon administered intramuscularly is useful in reptiles (e.g., 30 mg·kg⁻¹ in lizards), and isoflurane administered as gas is useful in birds (e.g., 2% in air for pigeons). Refer to the published literature³⁰⁻³² for a full overview of available anesthetics across species.

1.2. Test reflexes in the animal to confirm an optimal level of anesthesia. Ensure that the animal is completely motionless during the procedure as the flow-enhanced ultrasound procedure is sensitive to motion noise.

1.2.1. Too deep anesthesia can alter blood flow patterns, so conduct a dose titration in the start-up phase of an experiment.

1.2.2. Increase the anesthesia dosage in steps and observe blood flow in the eye aided by simple brightness mode (B-mode) ultrasound.

NOTE: An optimal level of anesthesia is obtained when the animal is motionless (except respiration) with visible ocular blood flow.

1.3. If the type/dose of anesthetic is not permissive for respiratory movements, then ensure adequate ventilation of the animal, e.g., using an air pump to oxygenate the water for aquatic species or a ventilator for air-breathing species.

1.4. Position the animal in a posture that allows direct access from above to the eye.

NOTE: Depending on species, this can be in either a supine or lateral position. It can be useful to construct a simple holding device using a small piece of non-reactive metal (e.g., stainless steel) and loose rubber bands (see **Figure 1**).

1.5. Place appropriate ultrasound medium on the eye of the animal. If scaled eyelids (ultrasound impermeable) cover the eye, then displace these gently with a cotton swab.

NOTE: For aquatic species, the best ultrasound medium is clean tank water in which the animal usually lives. For terrestrial species, a generous amount of ultrasound gel ensures free movements and imaging of the ultrasound transducer (i.e., linear array probe) across the entire surface of the eye. Vet ointment on the contralateral eye is required for terrestrial species.

2. 2D and 3D ocular ultrasound image acquisition

2.1. Position the ultrasound transducer medial to the eye in either a dorsal/ventral or rostral/caudal orientation depending on desired image orientation.

2.2. In B-mode, with a maximum depth of field, image the medial and deepest portion of the eye and make sure that all structures of interest are visible in the image field.

NOTE: In some species, the crystalline lens takes up a comparatively large proportion of the vitreous humor, which may absorb the ultrasound, especially at higher frequencies.

2.3. Slowly translate the transducer to each side while inspecting the real-time images. Make sure all structures of interest are visible in the image field; if not, switch to a transducer with a lower frequency and larger depth of field.

NOTE: The following center frequencies allow for the following maximum depth of field: 21 MHz: 3 cm, 40 MHz: 1.5 cm, 50 MHz: 1 cm (see **Table 1**). However, these maximum depth of field values can be markedly lower if the eye contains calcified or other ultrasound impermeable structures.

2.4. Adjust image depth, depth offset (distance from the top of the image to the structure of interest), image width, as well as number and position of focal zones to cover the desired region of interest in all three spatial dimensions (e.g., 1 cm image depth, 2 mm depth offset, 1 cm image width, one focal zone).

NOTE: Although specific naming of buttons that adjust these parameters may vary between ultrasound systems, most systems will have buttons with logical names for these adjustments. These image parameter settings usually affect the range of possible temporal resolutions of the ultrasound acquisition.

2.5. Set frame rate in the range of 50–120 frames·s⁻¹.

NOTE: The temporal resolution (i.e., the time interval between successive B-scans) must be adequate to display large pixel intensity variability in imaged blood vessels, i.e., the temporal resolution must not be too high. On the other hand, to complete a full 3D recording of the eye in a reasonable time, temporal resolution cannot be too low. A temporal resolution ranging from 50–120 frames·s⁻¹ is usually adequate for the flow-enhanced procedure in most species. On some ultrasound systems, this desired temporal resolution can be obtained by switching between the “general imaging” (high spatial/low temporal resolution) and “cardiology” (low spatial/high temporal resolution) modes.

2.6. Adjust 2D gain to a level (~5 dB), so anatomical structures are only just visible in the B-mode acquisition to increase the signal-to-noise ratio in the subsequent flow-enhanced reconstruction.

2.7. To acquire a 2D flow-enhanced image at a single slice position, translate the transducer to this position and continue at step 3.1.

2.8. To acquire a 3D recording of an entire region of interest, e.g., the retina, translate the transducer to one extreme of the region of interest.

2.8.1. To determine the exact position of the extreme end of the region of interest, increase the 2D gain briefly.

2.8.2. After correct transducer placement is complete, lower the 2D gain before recording to ensure maximal signal-to-noise ratio in the subsequent flow-enhanced reconstruction.

2.9. For each step (slice) in the 3D recording, acquire ≥ 100 frames (optimally ≥ 1000 frames).

2.10. Using a micromanipulator or build-in transducer motor, translate the transducer across the entire region of interest in steps of, e.g., 25 μm or 50 μm (remember to note the step size) and repeat the ≥ 100 frames acquisition for each step.

2.11. Euthanize the research animal according to the animal care guidelines of the institution.

3. Flow-enhanced image reconstruction

3.1. Export the recordings into digital imaging and communications in medicine (DICOM) file format (little-endian).

3.2. To produce a single flow-enhanced image based on a ≥ 100 frames (T) cine recording, calculate the standard deviation on pixel level ($STD(x,y)$) using the formula:

$$STD(x,y) = \left[\frac{1}{T} \sum_{t=1}^T ((I_t(x,y) - \bar{I}_t(x,y))^2) \right]^{\frac{1}{2}}$$

Where $I_t(x,y)$ is the intensity of the pixel at the (x,y) pixel coordinate at time t , and $\bar{I}_t(x,y)$ is the arithmetic mean value of I over time.

3.3. Repeat step 3.2 for each slice in the 3D recording.

3.4. To automate the STD-calculation and image reconstruction process for multiple slices in a 3D recording, conduct this operation in batch mode using, e.g., ImageJ and the supplementary macro script (**Supplementary File 1**).

3.5. Combine all reconstructed slices into one image stack (**Images to Stack** command in ImageJ).

3.6. Specify slice thickness from the step size used during acquisition (**Properties** command in ImageJ).

3.7. Save the image stack as a 3D TIF file.

NOTE: Flow-weighted three-dimensional recordings of ocular blood vessels can subsequently be used to create volume renderings and build digital and physical anatomical models of vascular

structures of the eye. These image processing options are outside the scope of this protocol; refer to the previously published articles for more details^{33–35}.

REPRESENTATIVE RESULTS:

The flow-enhanced ultrasound technique to image vascular beds of the eye can be applied in a range of species and has currently been used in 46 different vertebrate species (**Figure 1, Table 1**). The presence of nucleated red blood cells in non-adult-mammalian vertebrates provides positive contrast of flowing blood compared to static tissue in cine recordings (**Supplementary File 2**). However, when analyzed on a frame-by-frame basis, the clear distinction between blood and surrounding tissue is less obvious (**Figure 2A**). The blood flow enhancement procedure described in this protocol essentially compiles a multi-time point recording in 2D space (a slice made of T frames) into a single image in which the inherent signal value fluctuations in pixels positioned in flowing blood scores a higher standard deviation than surrounding static tissue, hence producing positive contrast (**Figure 2B**). To perceivably enhance the blood vessel contrast, Look Up Tables can be used to produce pseudocolor images (**Figure 2C**). In 3D acquisitions, multiple parallel slices with known spacing can be combined into 3D image data (**Supplementary File 3** and **Supplementary File 4**) that can be used for three-dimensional volume rendering (**Figure 2D**) and anatomical modeling (**Figure 2E** and **Supplementary File 5**). Doppler-based ultrasound imaging also provides the option to specifically image blood flow, however with less sensitivity than the described method (compare **Figure 2G** with **Figure 2H** and **Figure 2I**), and importantly not if blood flow orientation is directly or close to perpendicular to the direction of the sound wave. The flow-enhanced procedure described in this protocol is independent of the orientation of blood flow both in-plane and out-of-plane.

The flow-enhanced ultrasound procedure allows for blood flow imaging in a range of species with nucleated red blood cells (**Figure 3A–D**). Deep ocular vascular beds such as the choroid *rete mirabile* in some fish can be imaged if present in the species (yellow arrowhead in **Figure 2, Figure 3B, Figure 4**). The method is limited by the absence of nucleated red blood cells in adult mammals in which the flow enhancement procedure produces some degree of blood flow contrast but is not as distinct as in species with nucleated red blood cells (**Figure 3E,F**).

Flow-enhanced ultrasound is sensitive to motion noise, and, e.g., respiratory movements can cause image blurring and artifacts such as tissue border enhancement (**Figure 4A–C, Supplementary File 6**). Prospective or retrospective gating can be used to adjust for motion noise (**Figure 4D,E**).

FIGURE AND TABLE LEGENDS:

Figure 1: Examples of the variety of species suitable for flow-enhanced ultrasound imaging of ocular vasculature. (A) Goldfish (*Carassius auratus*). (B) Siberian sturgeon (*Acipenser baerii*). (C) European seabass (*Dicentrarchus labrax*). (D) Clown featherback (*Chitala ornata*). (E) Crucian carp (*Carassius carassius*). (F) Embryonic domestic chicken (*Gallus gallus domesticus*). It can be useful to construct a simple holding device using a non-reactive metal weight and loose rubber bands (A,C,D). Both large, immobile lab-based ultrasound imaging systems can be used for the procedure (A–D,F) as well as small field operative systems (E). When imaging small and highly

temperature-sensitive species that cannot be retained in a temperature-controlled water bath like embryonic birds, imaging can be performed while the sample is inside the incubator (F). This figure has been reprinted from bioRxiv³⁶.

Figure 2: Effect of flow enhancement on ocular ultrasound scans. (A) Examples of raw B-mode ultrasonographic images of the eye of a goldfish in a 1000 frame cine recording. Whereas blood flow can be observed in the cine recording (Supplementary File 2) it is difficult to see in static frames. (B) Flow-enhanced grayscale image (same slice as in A). Both retinal and post-retinal vascular beds are enhanced. (C) Pseudo-colored version of the image in B with ImageJ Fire Look Up Table. (D) Volume-rendered display of blood flow in the eye of the same goldfish as in A–C, based on 3D acquisition. (E) Two-segment (retinal and post-retinal vessels) anatomical model of eye in A–D (for interactive model see supplementary material 5). (F–I) Raw B-mode ultrasonographic image of the eye of another goldfish (F) comparing color Doppler based flow imaging (G) to the flow-enhanced methods described in this protocol (H–I, note I is an overlay of H on F). Green arrows indicate retinal vessels, yellow arrowheads indicate the choroid *rete mirabile*. This figure has been reprinted from bioRxiv³⁶.

Figure 3: Representative examples of flow-enhanced ocular ultrasound images in a variety of vertebrate species. (A) Senegal bichir (*Polypterus senegalus*). (B) Red-bellied piranha (*Pygocentrus nattereri*). (C) Green iguana (*Iguana iguana*). (D) Embryonic (day 18) domestic chicken (*Gallus gallus domesticus*). (E) House mouse (*Mus musculus*). (F) Brown rat (*Rattus norvegicus*). In species with nucleated red blood cells, the flow-enhancement procedure yields useful images of ocular blood flow (A–D), whereas in adult mammals (enucleated red blood cells), it produces only limited contrast between flowing blood and surrounding tissue (E–F). Green arrows indicate retinal vessels; blue arrowheads indicate post-retinal vessels such as the choriocapillaris; yellow arrowheads indicate choroid *rete mirabile*. In the late embryonic domestic chicken, blood flow in the pecten oculi can be observed (lower green arrow in F). This figure has been reprinted from bioRxiv³⁶.

Figure 4: Respiratory movements induce motion noise that can be alleviated by retrospective gating. (A–B) Example of respiratory movements in the eye of a European plaice (*Pleuronectes platessa*). The red dot is at the same image coordinate in A (slice 54/410) and B (slice 92/410), but it can be observed that the eye has shifted position (see also cine recording in supplementary material 6). (C) Attempt to perform the flow-enhancement operation on the full 410 frames recording fails due to motion noise. Tissue borders are artificially enhanced due to movements. (D) retrospective gating operation based on normalized signal intensity (SI) at the red dot in A–B. Only frames with normalized SI > 50 (in total 38 frames), i.e., indicating that the eye is at the same position as in B, are included for the flow-enhancement procedure. (E) Resulting image of retrospectively gated flow-enhancement procedure. Compare with C. In the gated image, artificial border enhancement is avoided, and blood flow in the choroid *rete mirabile* (yellow arrowhead) can be observed. This figure has been reprinted from bioRxiv³⁶.

Table 1: List of species on which the flow-enhanced ultrasound technique to image ocular blood flow has been used. The applicability of the method is based on the ability to produce a contrast-

rich representation of vascular beds compared to the static background. This table has been reprinted from bioRxiv³⁶.

Supplementary File 1: Macro script to automate flow-enhancement calculations. The script is written in IJ1 Macro language and can be executed both using the ImageJ macro function (for single slice recording) or the ImageJ Batch Process (for multiple slice 3D recording). This file has been reprinted from bioRxiv³⁶.

Supplementary File 2: Raw B-mode cine recording on the eye of a goldfish (*Carassius auratus*). Blood flow can be observed as the video is playing, but not on a single frame as in **Figure 2A**. This file has been reprinted from bioRxiv³⁶.

Supplementary File 3: Slice video through the eye of a goldfish (*Carassius auratus*) of blood flow-enhanced sections. This file has been reprinted from bioRxiv³⁶.

Supplementary File 4: Three-dimensional TIF file of the flow-enhanced eye of goldfish (*Carassius auratus*). Images have been binned by 3 x 3 x 3 to minimize file size (27-fold reduction in spatial resolution and file size). This file has been reprinted from bioRxiv³⁶.

Supplementary File 5: Interactive 3D model of pre- and post-retinal vessels in the eye of a goldfish (*Carassius auratus*). This file has been reprinted from bioRxiv³⁶.

Supplementary File 6: Raw B-mode cine recording on the eye of a European plaice (*Pleuronectes platessa*). Note respiratory movements. This file has been reprinted from bioRxiv³⁶.

DISCUSSION

Vascular imaging using flow-enhanced ultrasound provides a new method for non-invasive imaging of the vasculature of the eye that offers several advantages over present techniques but has its intrinsic limitations. The primary advantage of flow-enhanced ultrasound is the ability to generate ocular angiographies with a depth of field that exceeds the retinal pigment epithelium, which limits the depth of field in optical techniques. In ultrasound imaging, spatial resolution and depth of field are ultimately determined by the ultrasound transducer frequency, where higher frequencies increase the spatial resolution, but at the expense of a shallower depth of field, thus the choice of transducer frequency introduces a tradeoff between image depth and spatial resolution. In our experience, optimal retinal ultrasound imaging is achieved using high-frequency ultrasound transducers (≥ 50 MHz) in small eyes with image depths of <1 cm and lower frequency transducers (20–40 MHz) in larger eyes with image depths of 1.5–3.0 cm. For a 3D ultrasound scan, the resolution of the additional slice-dimension is set by the step size between scans in the stack of 2D ultrasound scans. In our experience, it is difficult to conduct a 3D scan with a step size smaller than 20 μm .

Flow-enhanced 2D ultrasound has a high temporal resolution. Ideally, ≥ 1000 frames per image are required for flow-enhanced vascular imaging, so at least 8 s are required per image scan. The

temporal resolution is significantly reduced when performing 3D flow-enhanced ultrasounds, where the scanning time increases with the number of images in the 3D stack of scans. Given the high temporal resolution, the flow-enhanced 2D ultrasound workflow shows strong potential as a method for identifying temporal changes in relative blood flow velocities and blood flow distribution during experimental manipulation. Thus, future studies can use the workflow to identify how altered environmental conditions (e.g., temperature, pO_2 , pCO_2) or pharmacological administration affect blood flow in the eye and other organs.

The ultrasound workflow relies on the positive contrast of nucleated red blood cells from most non-mammalian vertebrates. Thus, the enucleated red blood cells of adult mammals and some salamander species³⁷ provide too little contrast to effectively enhance blood flow using the present workflow (**Figure 3E,F**). In traditional ultrasound workflows, vascular injection of microbubbles provides high enough contrast to identify the vasculature in mammals³⁸, which has been used to generate vascular angiographies of the retrobulbar vessels within the rat eye³⁹. However, the microbubbles burst within minutes, so the generation of 3D angiographies requires successive microbubble injections.

Flow-enhanced ultrasound depends on sequential recordings in the same position of the eye, so the technique is not possible in awake animals, where minor random movements may offset the image and undermine flow-enhancement calculations. Thus, the present method must be performed under proper anesthesia for immobilization to enhance image quality by reducing random movements. However, regular movements of the eye that occur during regular respiratory movements can be offset by prospectively or retrospectively gating to the ventilation pattern of the animal, so only scan recording from the same time interval within the ventilation cycle is used in the data analysis. While the retrospective gating approach to offset ventilatory movements of the image significantly improves the image stability, it pronouncedly reduces the number of frames included in calculating the standard deviation of signal intensity leading to a decrease in signal-to-noise ratio (compare **Figure 4E** to **Figure 2C** and **Figure 2I**). This effect is alleviated using prospective gating at the ultrasound scanner, in which image data is only acquired when the animal is in the desired phase of respiration. However, this causes a marked increase in acquisition time if the desired number of frames ≥ 1000 must be acquired.

We see multiple applications in zoological and veterinarian research for the flow-enhanced ultrasound workflow to map the physiology and anatomy of the eye's vasculature. The vasculature of ray-finned fishes, mammals, and birds are relatively well-described^{1,3,4,8,9,12,15,40}, but this is not the case for non-bony fishes (jaw-less vertebrates and chondrichthyans), amphibians, and reptiles, that represent their respective earlier diverging sister groups. Implementing flow-enhanced ultrasound on these poorly understood animal groups and integrating these data with knowledge on the more well-studied groups will provide fundamental insight into the evolution of the vasculature of the vertebrate eye. Because the eye's vasculature is similar in closely related species⁴, such detailed information on the ocular vasculature in a broad range of species will provide a point-of-reference for veterinarians to identify malformations in the eye's vasculature due to developmental defects, diseases, or physical injuries. Furthermore, the ability to acquire 2D blood flow information with a high spatiotemporal

resolution provides the means for quantifying pharmacokinetic effects on blood flow distribution in deep vascular beds, with vast applications in drug development and testing. Future studies on this technique should focus on identifying injectable compounds that enhance the contrast of blood in species with enucleated red blood cells, which will expand the applicability of this technique to mammals with vast applications in biomedical research and clinical diagnostics of vascular dysfunction in the eye and other deep vascular beds.

ACKNOWLEDGMENTS

This work has received funding from the Carlsberg Foundation (CF17-0778; CF18-0658), the Lundbeck Foundation (R324-2019-1470; R346-2020-1210), the Velux Foundations (00022458), The A.P. Møller Foundation for the Advancement of Medical Science, the European Union's Horizon 2020 research and innovation program under the Marie Skłodowska-Curie grant agreement (No. 754513), and The Aarhus University Research Foundation.

DISCLOSURES

The authors declare that no completing interests exists.

REFERENCES

1. Yu, C. Q., Schwab, I. R., Dubielzig, R. R. Feeding the vertebrate retina from the Cambrian to the Tertiary. *Journal of Zoology*. **278** (4), 259–269 (2009).
2. Yu, D. Y., Cringle, S. J. Oxygen distribution and consumption within the retina in vascularised and avascular retinas and in animal models of retinal disease. *Progress in Retinal and Eye Research*. **20** (2), 175–208 (2001).
3. Country, M. W. Retinal metabolism: A comparative look at energetics in the retina. *Brain Research*. **1672**, 50–57 (2017).
4. Damsgaard, C. et al. Retinal oxygen supply shaped the functional evolution of the vertebrate eye. *Elife*. **8**, (2019).
5. Buttery, R. G., Hinrichsen, C. F. L., Weller, W. L., Haight, J. R. How thick should a retina be? A comparative study of mammalian species with and without intraretinal vasculature. *Vision Research*. **31** (2), 169–187 (1991).
6. Ames, A., Li, Y., Heher, E., Kimble, C. Energy metabolism of rabbit retina as related to function: high cost of Na⁺ transport. *The Journal of Neuroscience*. **12** (3), 840–853 (1992).
7. Chase, J. The Evolution of retinal vascularization in mammals: A comparison of vascular and avascular retinae. *Ophthalmology*. **89** (12), 1518–1525 (1982).
8. Johnson, G. L. Ophthalmoscopic studies on the eyes of mammals. *Philosophical Transactions of the Royal Society of London. Series B, Biological Sciences*. **254** (794), 207–220 (1968).
9. Johnson, G. L. I. Contributions to the comparative anatomy of the mammalian eye, chiefly based on ophthalmoscopic examination. *Philosophical Transactions of the Royal Society of London. Series B, Biological Sciences*. **194** (194–206), 1–82 (1901).
10. Rodriguez-Ramos Fernandez, J., Dubielzig, R. R. Ocular comparative anatomy of the family Rodentia. *Veterinary Ophthalmology*. **16** (s1), 94–99 (2013).
11. Copeland, D. E. Functional vascularization of the teleost eye. *Current Topics in Eye Research*. **3**, 219–280 (1980).

- 438 12. Meyer, D. B. in *The Visual System in Vertebrates. Handbook of Sensory Physiology* Vol. 7
439 (ed F. Crescitelli), Springer, Berlin, Heidelberg (1977).
- 440 13. Potier, S., Mitkus, M., Kelber, A. Visual adaptations of diurnal and nocturnal raptors.
441 *Seminars in Cell & Developmental Biology*. **106**, 116–126 (2020).
- 442 14. Wittenberg, J. B., Wittenberg, B. A. Active secretion of oxygen into the eye of fish. *Nature*.
443 **194**, 106–107 (1962).
- 444 15. Damsgaard, C. Physiology and evolution of oxygen secreting mechanism in the fisheye.
445 *Comparative Biochemistry and Physiology*. **252A**, 110840 (2021).
- 446 16. Damsgaard, C. et al. A novel acidification mechanism for greatly enhanced oxygen supply
447 to the fish retina. *Elife*. **9**, (2020).
- 448 17. Wittenberg, J. B., Haedrich, R. L. The choroid rete mirabile of the fish eye. II. Distribution
449 and relation to the pseudobranch and to the swimbladder rete mirabile. *Biological Bulletin*. **146**
450 (1), 137–156 (1974).
- 451 18. Wittenberg, J. B., Wittenberg, B. A. The choroid rete mirabile of the fish eye. I. Oxygen
452 secretion and structure: comparison with the swimbladder rete mirabile. *Biological Bulletin*. **146**
453 (1), 116–136 (1974).
- 454 19. Berenbrink, M. Historical reconstructions of evolving physiological complexity: O₂
455 secretion in the eye and swimbladder of fishes. *Journal of Experimental Biology*. **210** (Pt 9), 1641–
456 1652 (2007).
- 457 20. Berenbrink, M., Koldkjaer, P., Kepp, O., Cossins, A. R. Evolution of oxygen secretion in
458 fishes and the emergence of a complex physiological system. *Science*. **307** (5716), 1752–1757
459 (2005).
- 460 21. Keane, P. A., Sadda, S. R. Retinal imaging in the twenty-first century: State of the art and
461 future directions. *Ophthalmology*. **121** (12), 2489–2500 (2014).
- 462 22. Yung, M., Klufas, M. A., Sarraf, D. Clinical applications of fundus autofluorescence in
463 retinal disease. *International Journal of Retina and Vitreous*. **2** (1), 12 (2016).
- 464 23. Ang, M. et al. Optical coherence tomography angiography: a review of current and future
465 clinical applications. *Graefe's Archive for Clinical and Experimental Ophthalmology*. **256** (2), 237–
466 245 (2018).
- 467 24. Spaide, R. F., Koizumi, H., Pozonni, M. C. Enhanced depth imaging spectral-domain optical
468 coherence tomography. *American Journal of Ophthalmology*. **146** (4), 496–500 (2008).
- 469 25. Shen, Q. et al. Magnetic resonance imaging of tissue and vascular layers in the cat retina.
470 *Journal of Magnetic Resonance Imaging*. **23** (4), 465–472 (2006).
- 471 26. Tan, G. X., Jamil, M., Tee, N. G., Zhong, L., Yap, C. H. 3D reconstruction of chick embryo
472 vascular geometries using non-invasive high-frequency ultrasound for computational fluid
473 dynamics studies. *Annals of Biomedical Engineering*. **43** (11), 2780–2793 (2015).
- 474 27. Ho, S., Tan, G. X. Y., Foo, T. J., Phan-Thien, N., Yap, C. H. Organ dynamics and fluid
475 dynamics of the HH25 chick embryonic cardiac ventricle as revealed by a novel 4D high-frequency
476 ultrasound imaging technique and computational flow simulations. *Annals of Biomedical*
477 *Engineering*. **45** (10), 2309–2323 (2017).
- 478 28. Dittrich, A., Thygesen, M. M., Lauridsen, H. 2D and 3D echocardiography in the Axolotl
479 (*Ambystoma Mexicanum*). *Journal of Visualized Experiments: JoVE*. **141**, e57089 (2018).
- 480 29. Jia, Y. et al. Split-spectrum amplitude-decorrelation angiography with optical coherence
481 tomography. *Optics Express*. **20** (4), 4710–4725 (2012).

30. Clarke, K. W., Trim, C. M., Trim, C. M. *Veterinary Anaesthesia E-Book*. Elsevier Health Sciences (2013).
31. Flecknell, P. *Laboratory Animal Anaesthesia*. Elsevier Science & Technology (2015).
32. West, G., Heard, D., Caulkett, N. *Zoo Animal and Wildlife Immobilization and Anesthesia*. John Wiley & Sons, Inc. (2014).
33. Lauridsen, H., Hansen, K., Nørgård, M. Ø., Wang, T., Pedersen, M. From tissue to silicon to plastic: three-dimensional printing in comparative anatomy and physiology. *Royal Society Open Science*. **3** (3), 150643 (2016).
34. Lauridsen, H. et al. Inside out: Modern imaging techniques to reveal animal anatomy. *PLoS One*. **6** (3), e17879 (2011).
35. Ruthensteiner, B., Heß, M. Embedding 3D models of biological specimens in PDF publications. *Microscopy Research and Technique*. **71** (11), 778–786 (2008).
36. Damsgaard, C., Lauridsen, H. Deep vascular imaging in the eye with flow-enhanced ultrasound. *bioRxiv*. 2021.06.04.447055 (2021).
37. Mueller, R. L., Ryan Gregory, T., Gregory, S. M., Hsieh, A., Boore, J. L. Genome size, cell size, and the evolution of enucleated erythrocytes in attenuate salamanders. *Zoology*. **111** (3), 218–230 (2008).
38. Greis, C. Quantitative evaluation of microvascular blood flow by contrast-enhanced ultrasound (CEUS). *Clinical Hemorheology and Microcirculation*. **49**, 137–149 (2011).
39. Urs, R., Ketterling, J. A., Tezel, G., Silverman, R. H. Contrast-enhanced plane-wave ultrasound imaging of the rat eye. *Experimental Eye Research*. **193**, 107986 (2020).
40. Walls, G. L. *The vertebrate eye and its adaptive radiation*. Cranbrook Institute of Science, Michigan (1942).

Figure 1

[Click here to access/download;Figure;Fig_1-01.jpg](#)

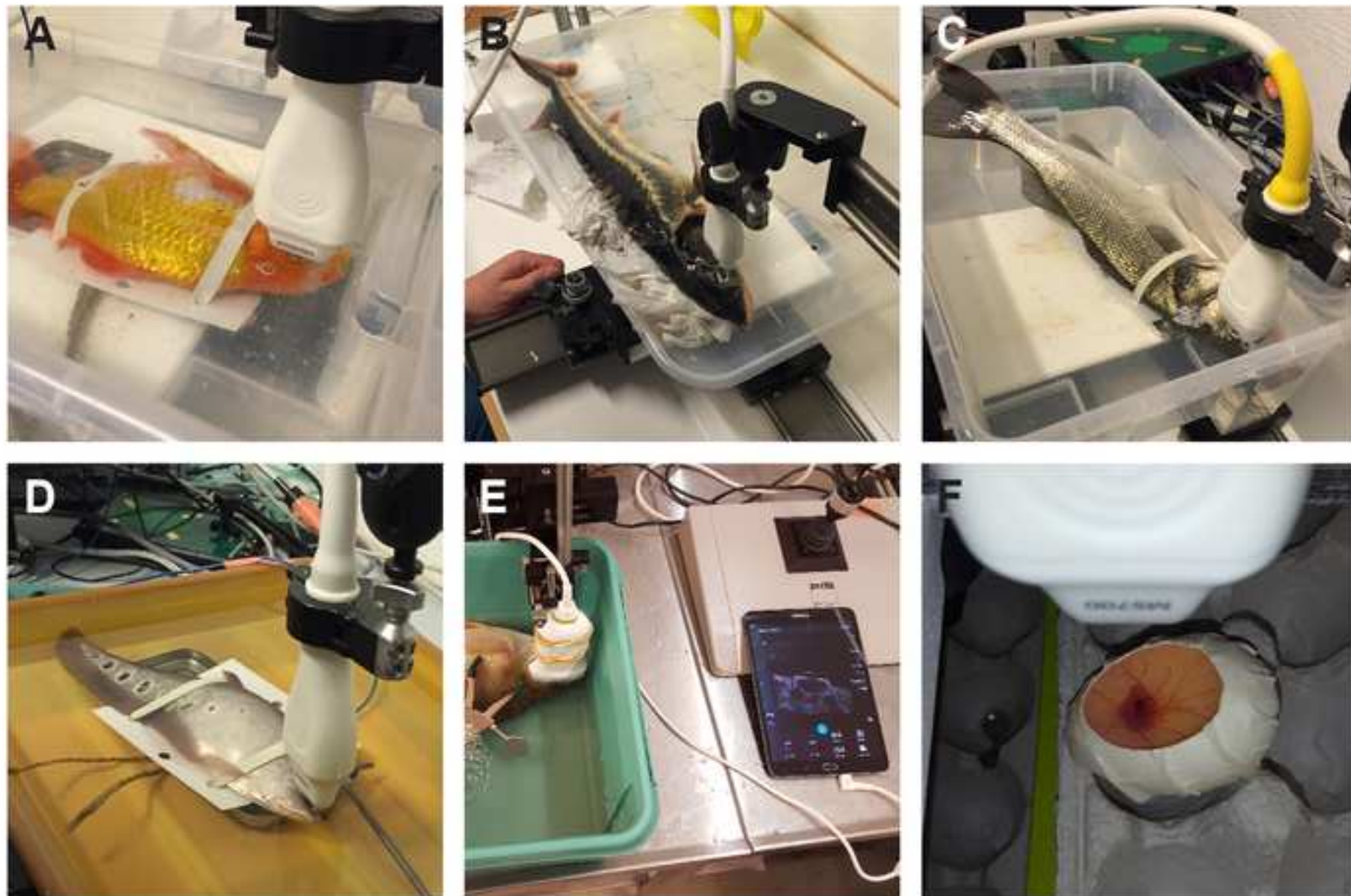


Figure 2

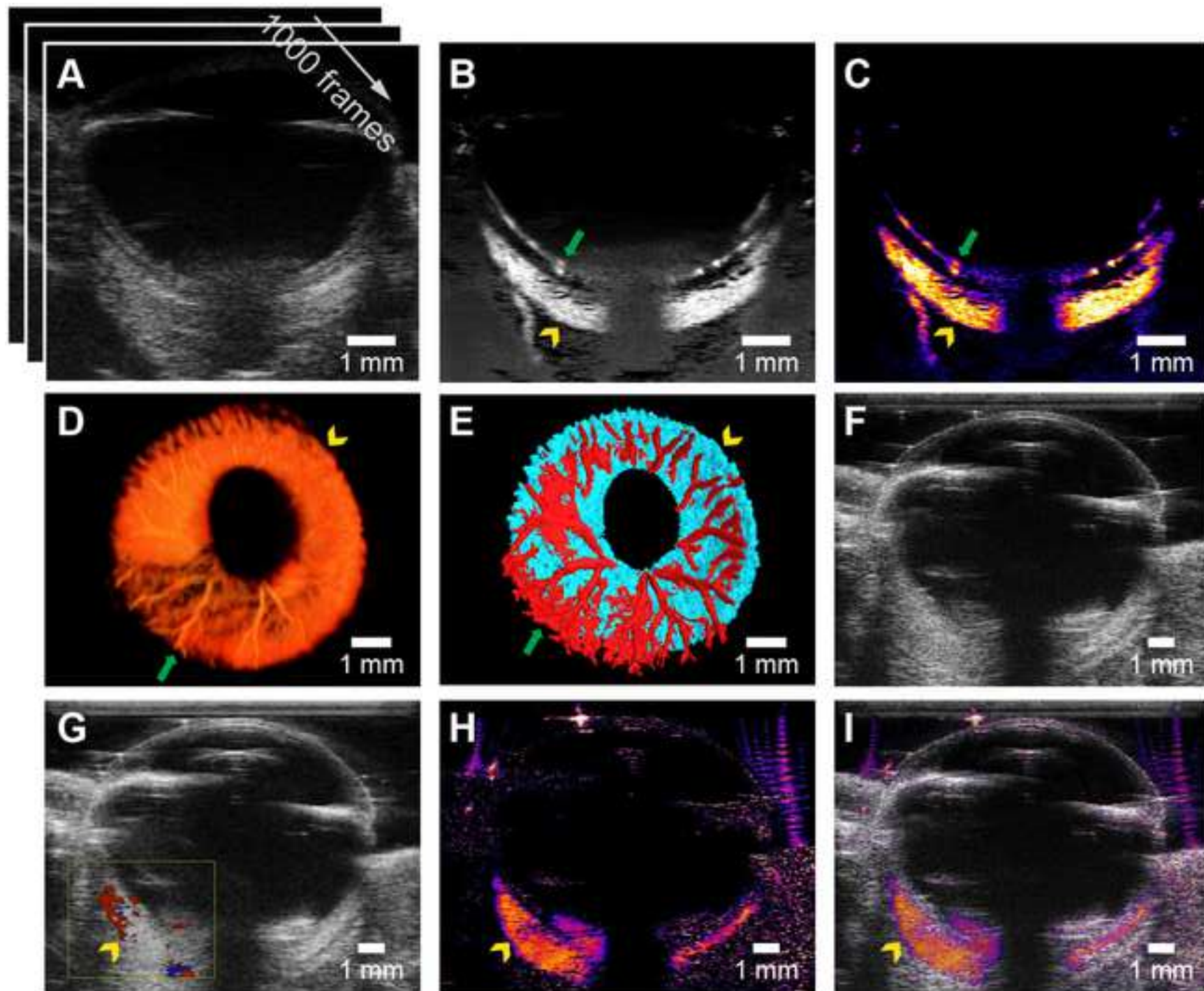


Figure 3

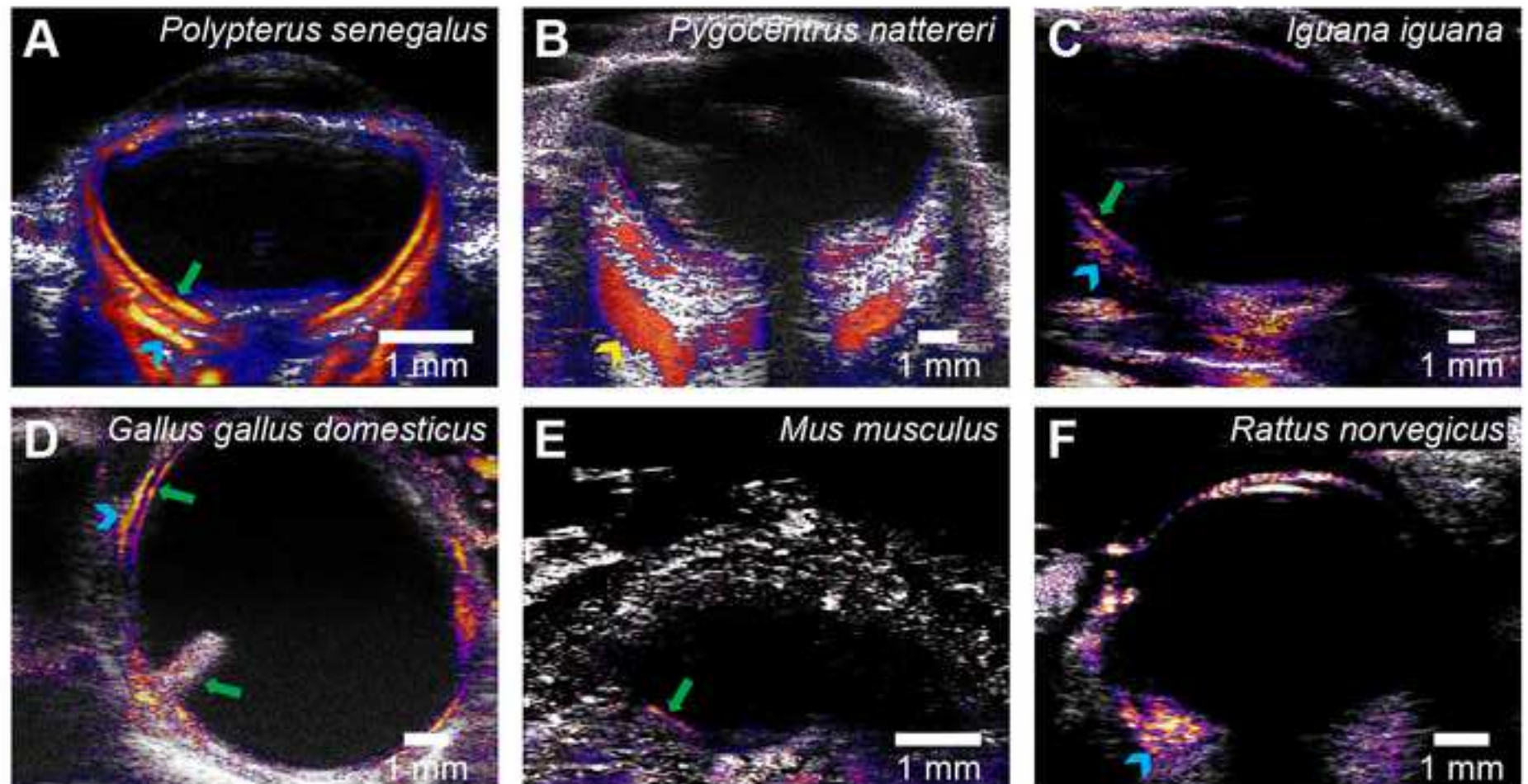
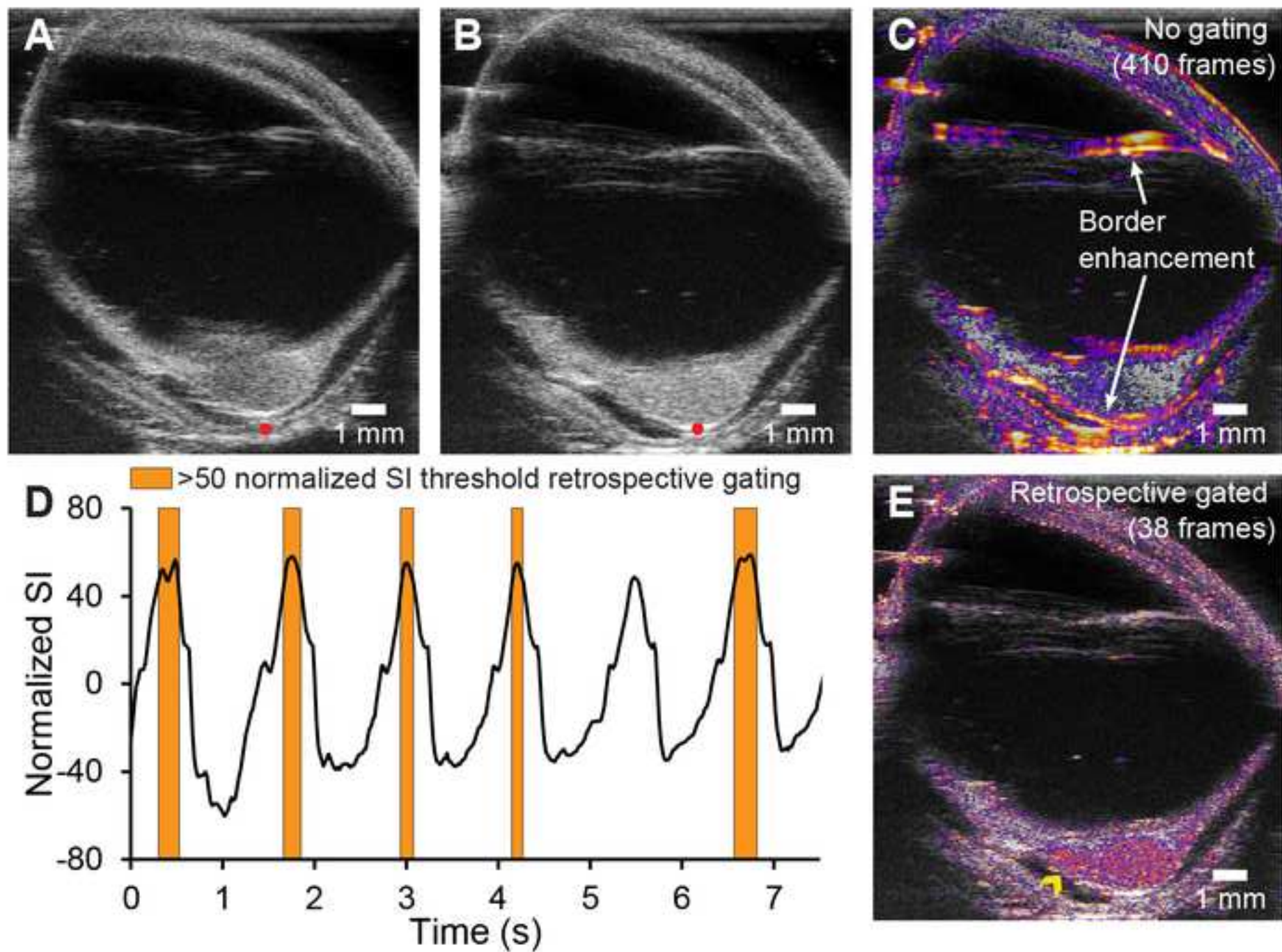


Figure 4

[Click here to access/download;Figure;Fig_4-01.jpg](#)



Clade	Common name	Binomial name
Actinopterii	Rice field eel	<i>Monopterus albus</i>
Actinopterii	Striped catfish	<i>Pangasianodon hypophthalmus</i>
Actinopterii	European plaice	<i>Pleuronectes platessa</i>
Actinopterii	Atlanti cod	<i>Gadus morhua</i>
Actinopterii	Senegal bichir	<i>Polypterus senegalus</i>
Actinopterii	Siberian sturgeon	<i>Acipenser baerii</i>
Actinopterii	Spotted gar	<i>Lepisosteus oculatus</i>
Actinopterii	Black ghost knifefish	<i>Apteronotus albifrons</i>
Actinopterii	Butterfly fish	<i>Pantodon buchholzi</i>
Actinopterii	Clown featherback	<i>Chitala ornata</i>
Actinopterii	European eel	<i>Anguilla anguilla</i>
Actinopterii	Goldfish	<i>Carassius auratus</i>
Actinopterii	Crucian carp	<i>Carassius carassius</i>
Actinopterii	Walking catfish	<i>Clarias batrachus</i>
Actinopterii	Fire eel	<i>Mastacembelus erythrotaenia</i>
Actinopterii	Rainbow trout	<i>Oncorhynchus mykiss</i>
Actinopterii	Perch	<i>Perca fluviatilis</i>
Actinopterii	European seabass	<i>Dicentrarchus labrax</i>
Actinopterii	Goldsinny wrasse	<i>Ctenolabrus rupestris</i>
Actinopterii	Three-spined stickleback	<i>Gasterosteus aculeatus</i>
Actinopterii	Freshwater angelfish	<i>Pterophyllum scalare</i>
Actinopterii	Obscure snakehead	<i>Parachanna obscura</i>
Actinopterii	Kuhli loach	<i>Pangio kuhlii</i>
Actinopterii	Elephantnose fish	<i>Gnathonemus petersii</i>
Actinopterii	Red-bellied piranha	<i>Pygocentrus nattereri</i>
Actinopterii	Mexican tetra (Surface ecotype)	<i>Astyanax mexicanus</i> (Surface ecotype)
Actinopterii	Mexican tetra (Micos cave ecotype)	<i>Astyanax mexicanus</i> (Micos cave ecotype)
Actinopterii	Mexican tetra (Pachón cave ecotype)	<i>Astyanax mexicanus</i> (Pachón cave ecotype)
Actinopterii	Blind cavefish	<i>Astyanax jordani</i>
Actinopterii	Humped rockcod	<i>Gobionotothen gibberifrons</i>
Actinopterii	Painted notie	<i>Lepidonotothen larseni</i>
Actinopterii	Yellowfin notie	<i>Lepidonotothen nudifrons</i>
Actinopterii	Black rockcod	<i>Notothenia coriiceps</i>
Actinopterii	Emerald rockcod	<i>Trematomus bernacchii</i>
Actinopterii		<i>Parachaenichthyes charcoti</i>
Actinopterii		<i>Vomeridens infuscipinnis</i>
Actinopterii	Blackfin icefish	<i>Chaenocephalus aceratus</i>
Actinopterii	Long-fingered icefish	<i>Cryodraco antarcticus</i>
Actinopterii	Jonah's icefish	<i>Neopagetopsis ionah</i>
Dipnoi	African lungfish	<i>Protopterus annectens</i>
Dipnoi	South American lungfish	<i>Lepidosiren paradoxa</i>
Amphibia	Mexican axolotl	<i>Ambystoma mexicanum</i>
Reptilia	Green iguana	<i>Iguana iguana</i>
Mammalia	House mouse	<i>Mus musculus</i>
Mammalia	Brown rat	<i>Rattus norvegicus</i>

Aves

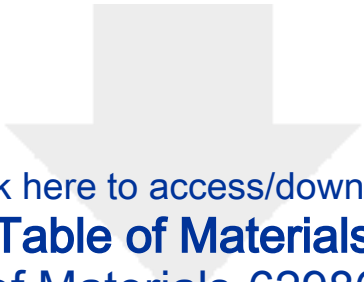
Domestic chicken

Gallus gallus domesticus

Type of ultrasound scan	Approximate axial length (m)	Ultrasound frequency
2D, stationary lab system	2.6	48
2D, stationary lab system	10.34	40
2D, stationary lab system	13.2	40
2D, stationary lab system	18.8	40
3D, stationary lab system	3.1	48
3D, stationary lab system	10.5	40
2D, stationary lab system	3.1	48
2D, stationary lab system	1.7	48
2D, stationary lab system	4.8	48
2D, stationary lab system	9.9	40
2D, stationary lab system	8.7	40
3D, stationary lab system	11.2	40
2D, stationary lab system	1.2	12
2D, stationary lab system	2.9	48
2D, stationary lab system	4	48
2D, stationary lab system	14.1	40
2D, stationary lab system	14	40
2D, stationary lab system	20.8	21
2D, stationary lab system	7.4	40
2D, stationary lab system	4.5	48
3D, stationary lab system	7.4	40
2D, stationary lab system	6.2	40
2D, stationary lab system	1.1	48
3D, stationary lab system	3.5	48
2D, stationary lab system	11.3	40
2D, stationary lab system	5	48
2D, stationary lab system	3.4	48
2D, stationary lab system	N/A	48
2D, stationary lab system	N/A	48
3D, portable system	4.8	50
2D, portable system	7.1	50
3D, portable system	5.5	50
3D, portable system	7.8	50
3D, portable system	5.2	50
3D, portable system	8.1	50
2D, portable system	9.2	50
3D, portable system	8.9	50
3D, portable system	8.7	50
3D, portable system	6.5	50
2D, stationary lab system	6.1	40
2D, stationary lab system	1.6	48
2D, stationary lab system	3.3	40
2D, stationary lab system	11.4	21
2D, stationary lab system	2.9	48
2D, stationary lab system	7	40

2D, stationary lab system	8.5	40
---------------------------	-----	----

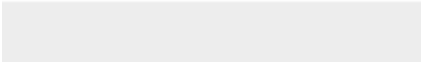
Frame rate (s-1)	Applicability of method
77	High
50	High
47	High
41	High
128	High
41	High
128	High
267	High
98	High
63	High
53	High
50	High
24	High
140	High
129	High
41	High
44	High
24	High
77	High
108	High
77	High
100	High
196	High
108	High
58	High
98	High
140	High
108	High
128	High
12	High
12	High
12	High
12	High
12	High
12	High
12	High
12	Low, few and rudimentary red blood cells
12	Low, few and rudimentary red blood cells
12	Low, few and rudimentary red blood cells
70	High
267	High
128	High
29	High
120	Low, enucleated red blood cells
65	Low, enucleated red blood cells



[Click here to access/download](#)

Table of Materials

Table of Materials-62986R2.xls



EDITORIAL COMMENTS

Changes to be made by the Author(s):

1. Please take this opportunity to thoroughly proofread the manuscript to ensure that there are no spelling or grammar issues. Please define all abbreviations at first use.

We have carefully read the manuscript and defined all abbreviations at first use.

2. To avoid confusion, please confirm the corresponding author (it's different in the manuscript and Editorial Manager).

Henrik Lauridsen will be the corresponding author on the final paper. Christian Damsgaard is listed as the corresponding author in Editorial manager, as the invitation was sent to him.

3. Please make sure the word count of the abstract is 150-300 words.

We made several minor text improvements in the abstract, which now is between 150 and 300 words.

4. Please highlight up to 3 pages of the Protocol (including headings and spacing) that identifies the essential steps of the protocol for the video, i.e., the steps that should be visualized to tell the most cohesive story of the Protocol. This will ensure that filming will be completed in one day. Remember that non-highlighted Protocol steps will remain in the manuscript, and therefore will still be available to the reader.

We would like the entire 3-page protocol to be used for the video.

5. The Protocol should contain only action items that direct the reader to do something. Please move the discussion about the protocol to the Discussion. The Protocol should be made up almost entirely of discrete steps without large paragraphs of text between sections. Please simplify the Protocol so that individual steps contain only 2-3 actions per step and a maximum of 4 sentences per step.

The protocol consists entirely of discrete steps without any discussing paragraphs.

6. Please note that your protocol will be used to generate the script for the video and must contain everything that you would like shown in the video. Please ensure you answer the "how" question, i.e., how is the step performed? Alternatively, add references to published material specifying how to perform the protocol action. There should be enough detail in each step to supplement the actions seen in the video so that viewers can easily replicate the protocol.

The protocol consists of detailed step that will supplement our actions seen in the video.

7. Given that your protocol discusses the use of this technique in different species, how will you film the video? Specific details will be required for the video and for readers to follow this protocol. Will you have multiple examples (different species)? If so, please look at the next point for details required for animal studies.

We will use goldfish (*Carassius auratus*) for the video recordings, as this species possess multiple types of retinal vasculature and is thus a highly illustrative example of the power of the ultrasound technique.

8. Being a video based journal, JoVE authors must be very specific when it comes to the humane treatment of animals. Regarding animal treatment in the protocol, please add the following information to the text:

a) Please include an ethics statement before all of the numbered protocol steps indicating that the protocol follows the animal care guidelines of your institution.

We have included an ethical statement as the first paragraph in the protocol.

b) What happens to the animals after the study? Please specify the euthanasia method without highlighting it.

We now mention that the animal is euthanized after ocular ultrasound.

c) Please mention how animals are anesthetized and how proper anesthetization is confirmed.

This is already described as a note to point 1.1.

d) Please specify the use of vet ointment on eyes to prevent dryness while under anesthesia.

We mention in the note to point 1.5 that vet ointment should be used in the contralateral eye of terrestrial species.

e) For survival strategies, discuss post-surgical treatment of animal, including recovery conditions and treatment for post-surgical pain.

f) Discuss maintenance of sterile conditions during survival surgery.

g) Please specify that the animal is not left unattended until it has regained sufficient consciousness to maintain sternal recumbency.

h) Please specify that the animal that has undergone surgery is not returned to the company of other animals until fully recovered.

Response to e)-h): Since we link the protocol to a specific animal experimentation protocol, where animals are euthanized during anesthesia, we do not describe post-experiment recovery. However, because the technique is non-invasive, post experiment recovery is possible.

9. Step 2.4: Please give more details (values, settings etc) and describe the button clicks, commands etc involved in this adjustment.

Specific values for ultrasound field of view (size of the image) are hard to provide because they depend on what the user is imaging. Name of buttons vary between ultrasound systems, but are usually logical (e.g. "Image depth" adjusts how deep the image is "Image width" how wide it is etc.). We have updated the note to step 2.4, specifying this point.

10. Steps 2.6-2.8, 3.4-3.5: HOW is the reader supposed to do these things? If you anticipate different instruments will require different steps, at least describe with your instrument, explain what is being done, explain all steps in detail, which will be helpful for the video and for readers. If image processing is outside the scope of the protocol, consider giving at least the values and settings to be used in a table and cite this table.

Response to 2.6: Gain adjustments is literally a button (usually a rotary knob) on all

ultrasound system. This will be clear to all users with basic training in ultrasound imaging.

Response to 2.7-2.8: Translating the transducer simply means to move (parallel displacement) the transducer from one position to another. This can hardly be explained in more detail.

Response to 3.4-3.5: We have added the ImageJ command name in parentheses. Also, in the note to step 3.3 we point the reader to Supplementary file 1 that contains an annotated ImageJ macro script exemplifying how calculations can be made in an imaging software.

11. Please include a scale bar for all images taken with a microscope to provide context to the magnification used. Define the scale in the appropriate Figure Legend.

All relevant images have scale bars.

12. Please sort the Materials Table alphabetically by the name of the material.
Done.

13. Files uploaded to the “Supplemental Files (as requested by JoVE)” section of your Editorial Manager account are only for JoVE’s internal use and will NOT be published with your article. If you would like your files to be available for download with your article, then please move them to the “Supplemental Code Files” section of your Editorial Manager account.

We have uploaded our videos to the Supplemental Code Files section of Editorial Manager.

REVIEWERS' COMMENTS

Reviewer #1:

Manuscript Summary:

The present study present a non-invasive ultrasound technique for generating three-dimensional angiographies in the eye without the use of contrast agents.

Major Concerns:

There are multiple applications in zoological and veterinarian research for the flow-enhanced ultrasound workflow to map the physiology and anatomy of the eye's vasculature. The present study merely applied this imaging approach in eyes across some different species, which jeopardize its attraction and novelty.

This imaging technique was originally designed to be applicable to a broad range of species, and we list 46 species of vertebrates in which this technique has been applied in Table 1. In the introduction and in the final paragraph of the discussion we describe how the technique can be used in zoological and veterinarian research.

The following might be take into account:

Clear comparison among different imaging strategies and the flow-enhanced workflow

The introduction contains a brief comparison between different retinal imaging techniques and how they compare to the presented flow-enhanced workflow.

However, it is now within the scope of this protocol-focused article to include a comprehensive comparison between these techniques.

Clarify the principle of the present flow-enhanced workflow and add illustration

Figure 2A-E presents the sequential steps in the flow-enhanced ultrasound protocol, and the six panels of figure 1 show an examples of the experimental setup.

Further study on future implementation of flow-enhanced ultrasound mapping of mammalian vasculatures replies on the microbubble and ultrasound

We have further elaborated on the mapping mammalian vasculatures by combining ultrasound and vascular microbubble injections. The text now reads:

“In traditional ultrasound workflows, vascular injection of microbubbles provides high enough contrast to identify the vasculature in mammals³⁶, which can be used to generate vascular angiographies of the retrobulbar vessels within the rat eye³⁷. However, the microbubbles burst within minutes, so generation of 3D angiographies requires successive microbubble injections. “

Reviewer #2:

Manuscript Summary:

This is an interesting paper that demonstrates a simple method for 2D and 3D imaging of ocular vasculature.

Major Concerns:

Line 50 and elsewhere: While the choriocapillaris is indeed posterior to the photoreceptors, the main cause of reduced OCT sensitivity is absorption of light by the retinal pigment epithelium. Note that OCT usually is based on near infrared light sources, which are not strongly absorbed by photoreceptors.

We have changed "photoreceptor" to "retinal pigment epithelium" in the introduction and the discussion.

Line 53: OCT systems can produce quite good images of the vasculature as deep as the choroid in clinical exams, particularly when using 'extended depth' technique or using 1µm swept-source..

Thank you for this great suggestion. We have revised the sentence, which now reads:

“Similar depth limitations are experienced in optical coherence tomography (OCT). This technique can generate high-resolution fundus angiographies using light waves at the technical expense of depth penetration²³, while the enhanced depth imaging OCT can visualize the choroid at the expense of retinal imaging quality²⁴. “

Line 104: At various points, the paper refers to the 'transducer.' From the figures, it would appear that this refers to a linear array probe. Please make it clear that a linear array probe was used rather than a mechanically scanned single-element transducer.

At first mention of the word transducer, we indicate that it is a linear array probe.

Line 120: Note that the crystalline lens, which is comparatively large in many species, strongly absorbs ultrasound, especially at higher frequencies.

We have added this suggestion as a note to point 2.2.

Line 137: By 'temporal resolution' I assume the author means the interval between successive B-scans, the inverse of the frame rate. Please state this for clarity.

We have now clarified that by “temporal resolution” we mean the time interval between successive B-scans.

Line 156: At some point, the authors should cite papers by Silverman and Urs in Exp Eye Res in 2021 and 2020 describing ocular blood flow imaging of the rat eye using ultrafast plane-wave methods and the advantages or limitations of their method compared to plane-wave.

We now mention the work of Urs et al's the third paragraph in the discussion when discussing the limitations of microbubble injections.

Line 169: The authors might note that this is similar in principle to the method used in OCT angiography (Jia et al, 2012) which is based on pixel decorrelation over multiple interrogations of each line or sight.

We have noted in the introduction that our methods applies similar principles as the OCT angiography and we have referred to the Jia et al 2012 paper.

Line 318: "Given the high temporal resolution, the flow-enhanced 2D ultrasound workflow shows strong potential as a method for identifying temporal changes in relative blood flow velocities and blood flow distribution during experimental manipulation." Systolic flow velocities may be on the order of 5-10 cm/sec depending on vessel and species. Depending on the ultrasound frequency, temporal resolution would probably need to be an order of magnitude higher to measure such velocities.

We respectfully disagree with the reviewer on this point. In the sentence, we explicitly say “relative blood flow velocities” i.e. not absolute values but changes following some kind of experimental manipulation. We have used frame rates (temporal resolution) in the range of 12 – 267 s⁻¹ in our ultrasound examination of eyes (see Table 1), although the system we primarily use can actually provide even higher temporal resolution (>400 s⁻¹) by decreasing spatial resolution and the size of the field of view. If we use the maximum systolic flow velocity value provided by the reviewer (10 cm s⁻¹) and the maximum temporal resolution we use in the manuscript (267 s⁻¹), then for every frame, blood cells will maximally have traveled 0.37 mm which is well within the field of view (usually in the range of centimeters) and would generate variation in pixel values over time that would provide contrast in a flow enhanced image, and could be used to detect relative changes if flow velocity was experimentally manipulated. We have not elaborated on this point in the revised manuscript.

Table 1 as presented is not very interesting. I would suggest adding a column indicating nucleated or non-nucleated red cells, possibly another column indicated approximate axial length of eye and perhaps ideal probe frequency. The ultrasound figures should include frequency of ultrasound probe and

frames/sec.

We have added two columns specifying the frequency of the ultrasound transducer and the axial diameter measured in the same animals.

Reviewer #3:

Manuscript Summary:

The authors are to be congratulated upon their interesting presentation of their findings to propose a novel non-invasive method for high resolution imaging of choroidal vessels. Their innovative technique can have potential implications for clinical use and I strongly recommend the acceptance of this manuscript for publication.

Major Concerns:

None

Minor Concerns:

None

Reviewer #4:

Manuscript Summary:

Conveys the proposed study succinctly, in a relevant area of work

Major Concerns:

none

Minor Concerns:

protocol for flow enhancement could be added

We have now described the sequential steps required for flow enhancement in ImageJ.



Click here to access/download
Supplemental Coding Files
Supplementary file_1.txt





[Click here to access/download](#)
Supplemental Coding Files
Supplementary file_2.mp4





[Click here to access/download](#)
Supplemental Coding Files
Supplementary file_3.mp4



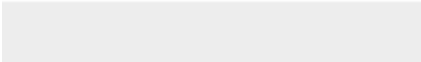



Click here to access/download
Supplemental Coding Files
Supplementary file_4.tif





[Click here to access/download](#)
Supplemental Coding Files
Supplementary file_5.pdf





[Click here to access/download](#)
Supplemental Coding Files
Supplementary file_6.mp4

